Optics Communications 392 (2017) 59–63

Contents lists available at ScienceDirect

Optics Communications

journal homepage: www.elsevier.com/locate/optcom

An extending broadband near-infrared absorption of Si-based deep-trench microstructures

Haigui Yang[a,*], Xiaoyi Liu[a,b], Jinsong Gao[a,b], Xiaoyi Wang[a], Hai Liu[a], Zhuo Zhang[a]

[a] Key Laboratory of Optical System Advanced Manufacturing Technology, Changchun Institute of Optics, Fine Mechanics and Physics, Chinese Academy of Sciences, Changchun 130033, China

[b] University of the Chinese Academy of Sciences, Beijing 100039, China

ARTICLE INFO

Keywords:
Silicon NIR absorption
Deep- trench microstructure
Surface plasmon polaritons
Plasmon cavity

ABSTRACT

We design and investigate numerically a Si-based deep-trench microstructure covered with continuous thin gold (Au) films. It breaks through the absorption limitation of Si material and greatly extends the near-infrared (NIR) absorption range to 1500 nm. By the simulated distributions of electric-field intensity, we observe clearly the excitation of surface plasmon polaritons and the standing wave resonance of plasmon cavity formed inside the deep trench, by which we explain the extending broadband NIR absorption well. We further discuss the influence of trench depth on the cavity mode and NIR absorption in detail. By combination of the proposed microstructures, it is a promising approach to realize an extending broadband and high NIR photoresponse in Si-based detectors.

1. Introduction

Compared with Ge and InGaAs semiconductor materials, developing a Si-based near-infrared (NIR) optoelectronic detector is more attractive because Si is the most economical, technologically sophisticated material with the highest crystal quality [1]. But Si has less absorption in the NIR region more than 1100 nm due to its wide band gap of 1.12 eV, which limits its optoelectronic applications within the visible and NIR region less than 1100 nm [2,3]. It is well known that surface plasmon polaritons (SPPs) based on metallic nanostructures can enhance the absorption by harvesting incident light and boost the performance of photoactive devices, such as solar cells [4,5], light emitting diodes [6,7] and photodetectors [8,9]. In particular, the extremely attractive point of SPPs is that it can break through the band-gap limitation and extend the intrinsic absorption region of materials, resulting in an extending photoresponse range of semiconductor detectors [10–15].

Recently Knight et al. have demonstrated that Si-based device was capable of absorbing and detecting light well below its band edge by combination of plasmonic metallic nanoantennas patterned on Si substrate [16]. Generally, photons coupled into a metallic nanoantenna excite SPPs, which can either decay radiatively into re-emitted photons or nonradiatively into energetic electrons, namely hot electrons [10,11,16,17]. When hot electrons cross the Schottky barrier formed at metal/Si interface before thermalization, they can be injected into the conduction band of Si, resulting in a photocurrent generation. In this case, the photoresponse range of Si is no longer limited by the band gap, and therefore Si-based device can realize the NIR photoresponse below its band edge. After that the extending NIR detection are also realized on Si-based device via random sized plasmonic nanoantennas and gratings [9,18–21]. According to these reports, the design of metallic nanostructures has a crucial influence on the extending photoresponse. For example, the internal quantum efficiency of Si-based detectors with metallic gratings is 0.2%, much higher than that (0.01%) with metallic nanoantennas because a stronger resonant absorption occurred in metallic grating structures [19].

In this study we design a Si-based deep-trench microstructure covered with continuous thin gold (Au) films. We demonstrate that this kind of microstructure allows for the excitation of broadband SPPs and the standing wave resonance of plasmon cavity formed inside the deep trench, consequently resulting in a greatly broadband and high NIR absorption within the extending range from 1000 nm to 1500 nm. We further discuss the cavity mode and NIR absorption in the microstructure with different trench depth by simulating the distributions of electric-field intensity (E). By combination of the proposed microstructures, it is expected that Si-based detectors are greatly potential to realize a broadband and high photoresponse in the extending NIR range from 1000 nm to 1500 nm.

* Corresponding author.
E-mail address: yanghg@ciomp.ac.cn (H. Yang).

http://dx.doi.org/10.1016/j.optcom.2017.01.041
Received 16 November 2016; Received in revised form 5 January 2017; Accepted 24 January 2017
Available online 31 January 2017

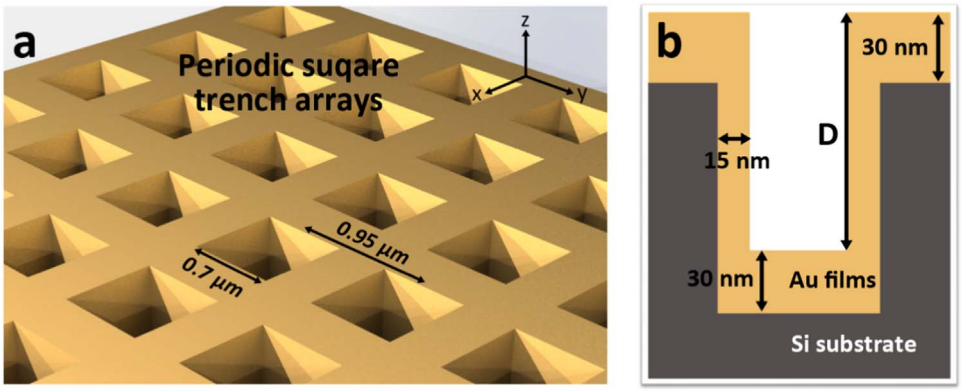

Fig. 1. Three-dimensional and cross-sectional diagrams of Si-based deep-trench microstructure.

2. Modeling calculation

A three-dimensional finite difference-time domain (3D-FDTD) algorithm is used to make a simulation study on the designed deep-trench microstructures. The three-dimensional and cross-sectional diagrams of Si-based deep-trench microstructure is given in Fig. 1. It is composed of periodically arranged square-trench arrays. The side length of square trench is 0.7 μm, and its period is 0.95 μm. The trench depth is D as a variable parameter. The top of the microstructure surface, the bottom and sidewalls of the deep trench are all covered with a layer of thin Au films. The Au film thickness on both top and bottom is 30 nm, and the sidewall inside the deep trench is 15 nm. Here, it is noted that we choose two different Au film thickness. This is because that when it is deposited on the deep-trench microstructure by a physical-vapor-deposition method such as thermal evaporation and magnetron sputtering, the thickness of Au film on the sidewall will be always thinner than that on the top surface due to the shadowing effect from oblique incident atoms. When the designed deep-trench microstructure is used to prepare a photodetector, it is helpful for the photocurrent extraction because the large-area continuous Au films on the surface can be acted as metal electrodes.

3. Results and discussions

Fig. 2 shows the NIR light absorption of D=2.4 μm. The absorption spectra are extracted by the formula of A=1-R-T, where A is absorptance, R is reflectance and T is transmittance. Obviously the deep-trench microstructure exhibits a very broadband and high absorption with a peak value of 98% and an average value of 82% in the NIR region from 1000 nm to 1500 nm. It is known that traditional Si has less absorption in the NIR region more than 1100 nm due to its wide band gap of 1.12 eV, while the designed Si-based microstructure breaks through the absorption limitation of Si material and greatly extends its NIR absorption range to 1500 nm. Fig. 3 shows the NIR light absorption as a function of D, from which we would like to illustrate how dominant the influence of D on both the band width and the intensity of NIR absorption is. When D=0.2 μm, the trench microstructure is very shallow, and a narrowband absorption with a peak value less than 60% is observed at 1150 nm. With a gradual increase in D, an exciting phenomenon occurs. The NIR absorption is enhanced, and more importantly, the absorption bandwidth is drastically broadened. The deeper the D is, the broader the absorption bandwidth becomes. It completely changes to a broadband absorption in the deep-trench microstructure from a narrowband absorption in the shallow-trench one. This indicates that D makes a crucial contribution to both the band width and the intensity of NIR absorption. In addition, Fig. 4 shows the influence of period size on the absorption of designed microstructure with D=1.2 μm. With an increase in the period size, the absorption bands shift to longer wavelengths gradually, which is a general phenomenon presented in many microstructures [16,22]. Simulation results indicate that the red-shift is mainly caused by the

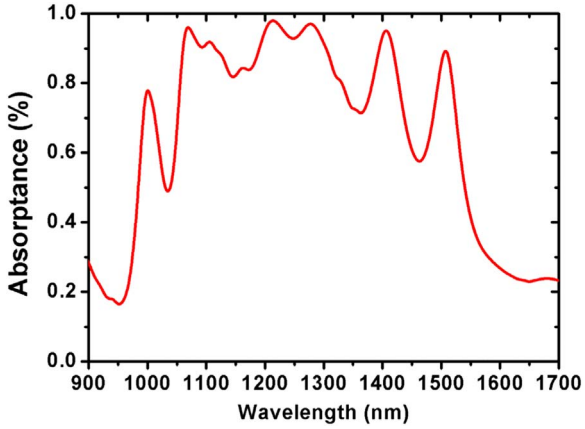

Fig. 2. NIR light absorption of Si-based deep-trench microstructure with D=2.4 μm.

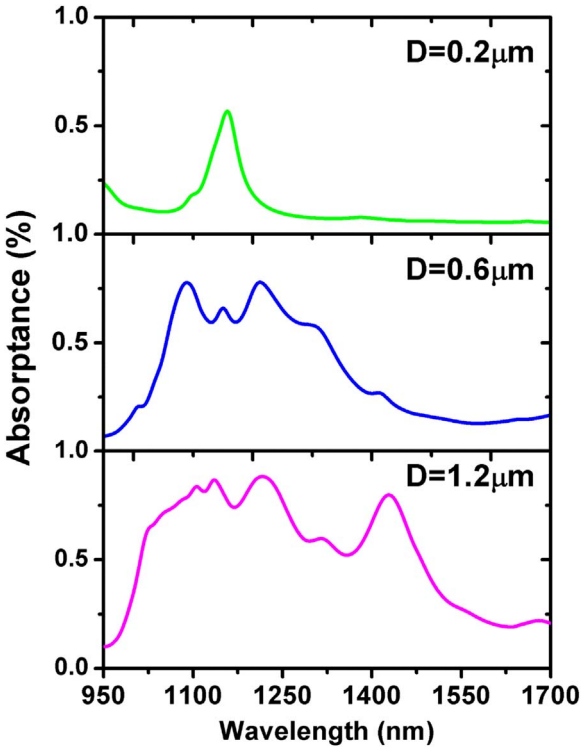

Fig. 3. NIR light absorption as a function of trench depth.

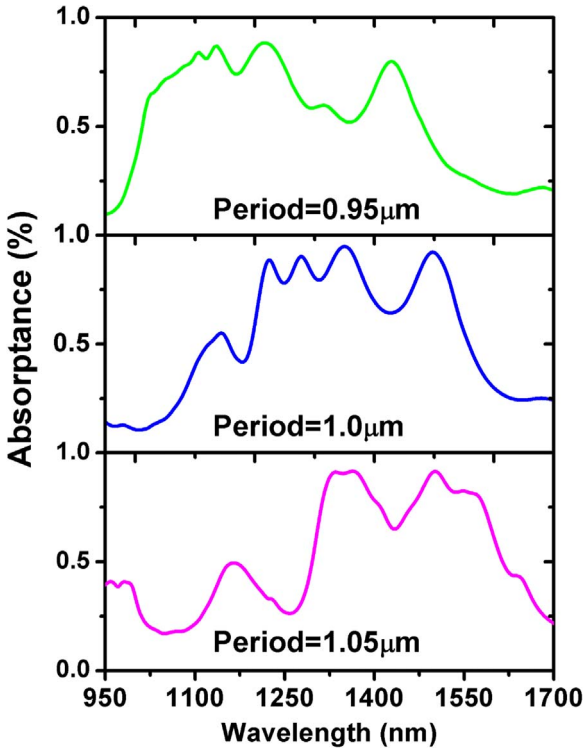

Fig. 4. The influence of period size on the absorption of designed microstructure with D=1.2 μm.

increased surface reflection in the shorter-wavelength region.

In order to clarify the origin of NIR absorption, and in particular the distinction between shallow and deep trench microstructures, we compare the electric-field (E) distributions in the trench microstructure with different D. Fig. 5 shows the cross-sectional E distributions at the incident wavelength of 1150 nm and 1250 nm when D=0.2 μm and 0.6 μm, where the color bars are consistent and the highlighted areas represent that E is stronger than others. The polarization direction of incident light is along the X axis. In the case of shallow-trench of D=0.2 μm, the microstructure only has a strong binding effect at the short wavelength of 1150 nm. It is worth noting that E mainly converges in the top interface and vertexes of shallow trench. While at long wavelength of 1250 nm, E convergence not only disappears in the top interface, but becomes relative weak in the vertexes. Thus it only exhibits a narrowband absorption in the shallow-trench microstructures of D=0.2 μm in Fig. 3. Completely different with shallow-trench microstructures, in the case of deep trench of D=0.6 μm, strong convergence of E distributes at 1150 nm not only in the top interface of shallow trench, but deeply inside the sidewall region of the trench. In particular, strong convergence of E inside the sidewall region becomes more dominant at 1250 nm. Thus it exhibits a broadband absorption in the deep-trench microstructures of D=0.6 μm in Fig. 3. By a comparison of the dependence of both absorption and E distributions on D in Fig. 3 and Fig. 5, we can conclude that the broadband and high absorption in the NIR region is mainly attributed to strong E convergence inside the sidewall region of deep trench.

In deep-trench microstructures, we consider that the SPP excitation at metal/dielectric interface leads to strong E convergence. SPPs excited in variety structures have been reported [23–26], which can confine energy of incident electromagnetic wave to a thin range near the metal/dielectric interface. The spatial compression of energy induces that the plasmonics have a high ability in light trapping [11,27]. Generally, SPP excitation contributes a narrow band absorption [16,18,19]. By contrast, in this study a very broadband absorption is achieved in deep-trench microstructures, which should be originated from the plasmon cavity effects formed inside the deep trench. In order to clarify this, in Fig. 6 we present the cross-sectional E distributions with a plasmon cavity behavior around 1250 nm, 1400 nm and 1500 nm in the deep trench of D=2.4 μm. Very different from the similar deep-trench microstructure reported by Liu et al. [28], the resonance phenomenon of multiple SPP cavity modes was not observed. Plasmon cavity is similar to the plane-wave cavity, except that plane-waves are replaced with SPPs [29–32]. The resonant modes of plasmon cavity are formed by the interference of forward and backward propagating waves and are determined by the dispersion relation of the waveguide and the phase shifts at each end [32]:

$$2k_{sp}h + \varphi_1 + \varphi_2 = 2m\pi$$

where k_{sp} is the wave vector of the surface plasmon wave, h is the length of the cavity, φ_1 and φ_2 are the phase changes at the top and bottom boundaries, and m is the resonance order. From this equation, we can see that the longer h is, the higher order resonant wave can be excited. E distributions in Fig. 6 from FDTD calculations visualize the characteristics of plasmon cavity, and it obviously exhibits a standing-wave resonance behavior of plasmon cavity. Similar standing-wave resonance of plasmon cavity has been studied by Zhu et. al. [33], which can offer the simultaneous excitation of broadband SPP modes and therefore an efficient plasmon-induced transparency. Bora et. al. also reported a plasmonic resonant nanocavities [32], resulting that additional harmonics can be excited at higher frequencies extending the absorbance range to multiple wavelengths.

It can be seen clearly from Fig. 6 that the shorter wavelength is, the higher order the standing wave becomes. The zeroth order standing wave is located around the longer wavelength of 1500 nm while the higher order around the shorter wavelength of 1400 nm and 1250 nm. Fig. 7 shows the cross-sectional E distributions in the trench of D=0.6 μm, 1.2 μm and 2.4 μm, respectively. All of them exhibit the zeroth order standing wave resonance of plasmon cavity, but the resonance wavelength is different. As D increases, the resonance wavelength of the zeroth order cavity mode becomes longer, and therefore higher order cavity modes are excited inside the deep trench (see Fig. 6). Contrarily, in the shallow trench of D=0.2 μm, the standing-wave resonance cannot be excited (see Fig. 5) due to too shallow depth. In another word, the deeper the D is, the higher order the cavity mode has. The deep-trench microstructures allow the existence of multiple SPP cavity modes, resulting in a broadband absorption. That is why the absorption bandwidth in Fig. 3 becomes broad greatly with D increasing. Because SPP is excited on metal films, when we removed the Au films on the sidewall region we found that SPP cannot be excited and standing wave resonance cannot be formed inside the deep trench like that with all Au films. In this case, the microstructures have a very weak ability to converge and trap the energy of incident light inside the deep trench. Thus, we believe that the standing wave resonance of plasmon cavity formed inside the deep trench contributes dominantly to the broadband high NIR absorption in the deep trench microstructures.

4. Conclusion

In summary, we have demonstrated an extending broadband NIR absorption by using a Si-based deep-trench microstructure covered with Au films. It breaks through the absorption limitation of Si and greatly extends its NIR absorption to 1500 nm. We found that the NIR absorption bandwidth and its intensity drastically increased when the trench became deeper. By an analysis of electrical-field distributions, we concluded that the broadband NIR absorption were mainly attributed to the excitation of SPPs and the standing wave resonance of plasmon cavity formed inside the deep trench. With an increase in the trench depth, higher order standing waves can be excited, resulting in a very broadband and high absorption with a peak value of 98% and an average value of 82% in the NIR region from 1000 nm to 1500 nm in the microstructures with the trench depth of 2.4 μm. By combination

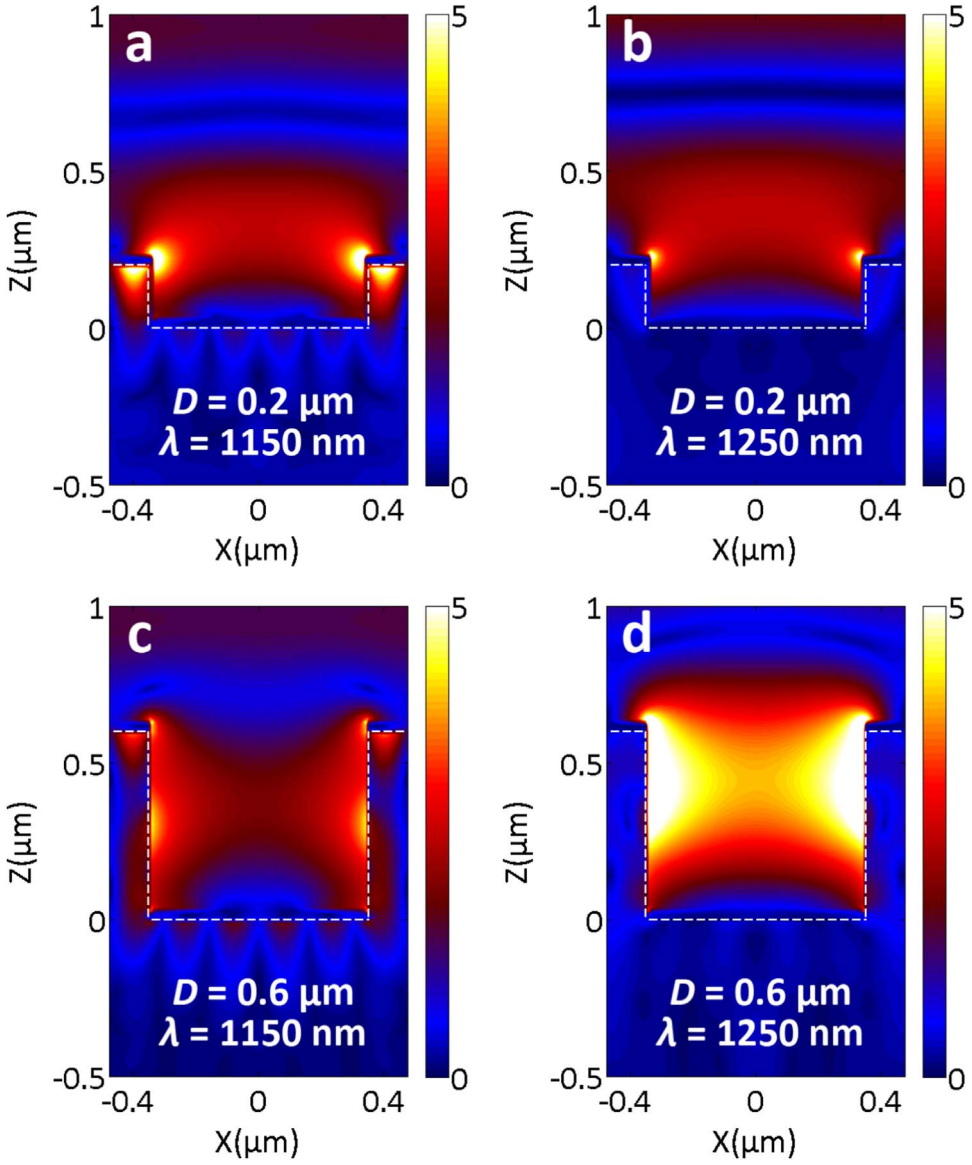

Fig. 5. A comparison of cross-sectional E distributions at the incident wavelength of 1150 nm and 1250 nm when D=0.2 μm and 0.6 μm. The color bars are consistent and the highlighted areas represent that E is stronger than others. (For interpretation of the references to color in this figure legend, the reader is referred to the web version of this article.)

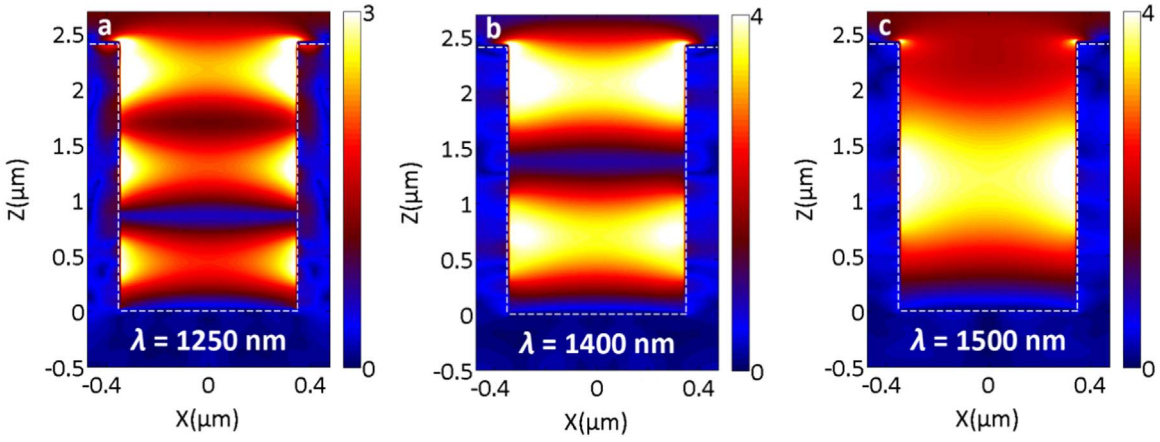

Fig. 6. Cross-sectional E distributions around 1250 nm, 1400 nm and 1500 nm in the deep trench of D=2.4 μm.

of the proposed microstructures, it is expected that Si-based detectors are greatly potential to realize a broadband and high photoresponse in the extending NIR region from 1000 nm to 1500 nm.

Acknowledgements

This project was supported by the National Natural Science

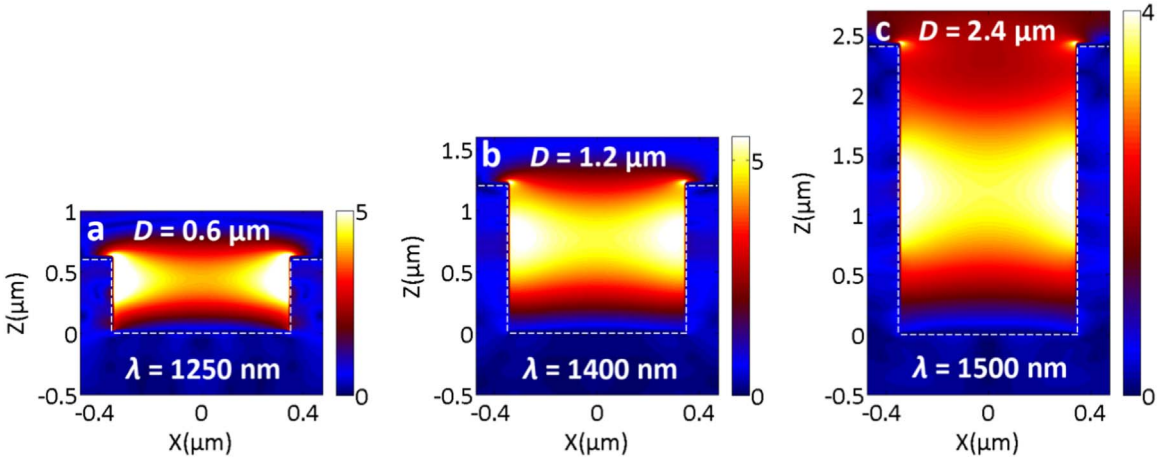

Fig. 7. Cross-sectional E distributions around 1250 nm for D=0.6 μm, 1400 nm for D=1.2 μm, and 1500 nm for D=2.4 μm.

Foundation of China (Nos. U1435210, 61306125, 61675199 and 11604329), the Science and Technology Innovation Project (Y3CX1SS143) of CIOMP, the Science and Technology Innovation Project of Jilin Province (Nos. 20130522147JH and 20140101176JC).

References

[1] Z.H. Huang, J.E. Carey, M.G. Liu, X.Y. Guo, E. Mazura, J.C. Campbellb, Microstructured silicon photodetector, Appl. Phys. Lett. 89 (2006) 033506.
[2] R. Younkin, J.E. Carey, E. Mazur, J.A. Levinson, C.M. Friend, Infrared absorption by conical silicon microstructures made in a variety of background gases using femtosecond-laser pulses, J. Appl. Phys. 93 (2003) 2626.
[3] M.J. Smith, M.J. Sher, B. Franta, Y.T. Lin, E. Mazur, S. Gradečak, Improving dopant incorporation during femtosecond-laser doping of Si with a Se thin-film dopant precursor, Appl. Phys. A 114 (2014) 1009.
[4] R.A. Pala, J. White, E. Barnard, J. Liu, M.L. Brongersma, Design of plasmonic thin-film solar cells with broadband absorption enhancements, Adv. Mater. 21 (2009) 3504.
[5] V.E. Ferry, L.A. Sweatlock, D. Pacifici, H.A. Atwater, Plasmonic nanostructure design for efficient light coupling into solar cells, Nano Lett. 8 (2008) 4391.
[6] K. Okamoto, I. Niki, A. Shvartser, Y. Narukawa, T. Mukai, A. Scherer, Surface-plasmon-enhanced light emitters based on InGaN quantum wells, Nat. Mater. 3 (2004) 601.
[7] K.Y. Yang, K.C. Choi, C.W. Ahn, Surface plasmon-enhanced energy transfer in an organic light-emitting device structure, Opt. Express 17 (2009) 11495.
[8] P.Y. Fan, K.C.Y. Huang, L.Y. Cao, M.L. Brongersma, Redesigning photodetector electrodes as an optical antenna, Nano Lett. 13 (2013) 392.
[9] M.A. Nazirzadeh, F.B. Atar, B.B. Turgut, A.K. Okyay, Random sized plasmonic nanoantennas on Silicon for low-cost broad-band near-infrared photodetection, Sci. Rep. 4 (2014) 7103.
[10] W. Li, J. Valentine, Metamaterial perfect absorber based hot electron photodetection, Nano Lett. 14 (2014) 3510.
[11] K.T. Lin, H.L. Chen, Y.S. Lai, C.C. Yu, Silicon-based broadband antenna for high responsivity and polarization-insensitive photodetection at telecommunication wavelengths, Nat. Commun. 5 (2014) 3288.
[12] M.K. Hedayati, M. Javaherirahim, B. Mozooni, R. Abdelaziz, A. Tavassolizadeh, V.S.K. Chakravadhanula, V. Zaporojtchenko, T. Strunkus, F. Faupel, M. Elbahri, Design of a perfect black absorber at visible frequencies using plasmonic metamaterials, Adv. Mater. 23 (2011) 5410.
[13] K. Aydin, V.E. Ferry, R.M. Briggs, H.A. Atwater, Broadband polarization-independent resonant light absorption using ultrathin plasmonic super absorbers, Nat. Commun. 2 (2011) 517.
[14] K. Du, Q. Li, Y. Lyu, J. Ding, Y. Lu, Z. Cheng, M. Qiu, Control over emissivity of zero-static-power thermal emitters based on phase-changing material GST, Light Sci. Appl. 6 (2017) e16194.
[15] K. Du, Q. Li, W. Zhang, Y. Yang, M. Qiu, Wavelength and thermal distribution selectable Microbolometers based on metamaterial absorbers, IEEE Photonics J. 7 (2015) 1.
[16] M.W. Knight, H. Sobhani, P. Nordlander, N.J. Halas, Photodetection with active optical antennas, Science 332 (2011) 702.
[17] R. Sundararaman, P. Narang, A.S. Jermyn, W.A. Goddard, H.A. Atwater, Design of plasmonic thin-film solar cells with broadband absorption enhancements, Nat. Commun. 5 (2014) 5788.
[18] M.W. Knight, Y.M. Wang, A.S. Urban, A. Sobhani, B.Y. Zheng, P. Nordlander, N.J. Halas, Embedding plasmonic nanostructure diodes enhances hot electron emission, Nano Lett. 13 (2013) 1687.
[19] A. Sobhani, M.W. Knight, Y.M. Wang, B. Zheng, N.S. King, L.V. Brown, Z.Y. Fang, P. Nordlander, N.J. Halas, Narrowband photodetection in the near-infrared with a plasmon-induced hot electron device, Nat. Commun. 4 (2013) 1643.
[20] Y. Qu, Q. Li, H. Gong, K. Du, S. Bai, D. Zhao, H. Ye, M. Qiu, Spatially and Spectrally Resolved Narrowband Optical Absorber Based on 2D Grating Nanostructures on Metallic Films, Adv. Opt. Mater. 4 (2016) 480.
[21] X. Chen, H. Gong, S. Dai, D. Zhao, Y. Yang, Q. Li, M. Qiu, Near-infrared broadband absorber with film-coupled multilayer nanorods, Opt. Let. 38 (2013) 2247.
[22] X.Y. Liu, J.S. Gao, H.G. Yang, X.Y. Wang, Si-based near-infrared narrowband absorber based on square Au patches, J. Opt. Soc. Am. B 33 (2016) 2149.
[23] M.R. Gadsdon, I.R. Hooper, A.P. Hibbins, J.R. Sambles, Surface plasmon polaritons on deep, narrow-ridged rectangular gratings, J. Opt. Soc. Am. B 26 (2009) 1228.
[24] A. Dhibi, M. Khemiri, M. Oumezzine, Theoretical study of surface plasmons coupling in transition metallic alloy 2D binary grating, Physica E 79 (2016) 160.
[25] J. Yang, F.F. Luo, T.S. Kao, X. Li, G.W. Ho, J.H. Teng, X.G. Luo, M.H. Hong, Design and fabrication of broadband ultralow reflectivity black Si surfaces by laser micro/nanoprocessing, Light Sci. Appl. 3 (2014) e185.
[26] L.L. Huang, X.Z. Chen, B.F. Bai, Q.F. Tan, G.F. Jin, T. Zentgraf, S. Zhang, Helicity dependent directional surface plasmon polariton excitation using a metasurface with interfacial phase discontinuity, Light Sci. Appl. 2 (2013) e70.
[27] Q. Sun, K. Ueno, H. Yu, A. Kubo, Y. Matsuo, H. Misawa, Direct imaging of the near field and dynamics of surface plasmon resonance on gold nanostructures using photoemission electron microscopy, Light Sci. Appl. 2 (2013) e118.
[28] X.Y. Liu, J.S. Gao, H.G. Yang, H. Liu, X.Y. Wang, Z.F. Shen, Near-infrared absorption enhancement mechanism investigations of deep-Trench silicon microstructures covered with gold films, Plasmonics 11 (2016) 1019.
[29] M. Qiao, R. Gordon, Surface plasmon microcavity for resonant transmission through a slit in a gold film, Opt. Express 16 (2008) 9708.
[30] K.Y. Wu, T. Rindzevicius, M.S. Schmidt, K.B. Mogensen, S.S. Xiao, A. Boisen, Plasmon resonances of Ag capped Si nanopillars fabricated using mask-less lithography, Opt. Express 23 (2015) 12965.
[31] Y. Huang, X. Zhang, E. Ringe, M.J. Hou, L.W. Ma, Z.J. Zhang, Tunable lattice coupling of multipole plasmon modes and near-field enhancement in closely spaced gold nanorod arrays, Sci. Rep. 6 (2016) 23159.
[32] M. Bora, E.M. Behymer, D.A. Dehlinger, J.A. Britten, C.C. Larson, A.S.P. Chang, K. Munechika, H.T. Nguyen, T.C. Bond, Plasmonic black metals in resonant nanocavities, Appl. Phys. Lett. 102 (2013) 251105.
[33] Y. Zhu, X.Y. Hu, H. Yang, Q.H. Gong, On-chip plasmon-induced transparency based on plasmonic coupled nanocavities, Sci. Rep. 4 (2014) 3752.